DIFFRACTIVE AND PHOTON-INDUCED PROCESSES AT THE LHC: FROM THE ODDERON DISCOVERY, THE EVIDENCE FOR SATURATION TO THE SEARCH FOR AXION-LIKE PARTICLES*

Christophe Royon

The University of Kansas, Lawrence, USA
christophe.royon@cern.ch

Received 18 March 2026, accepted 8 April 2026, published online 28 May 2026

We discuss first the discovery of the odderon by the TOTEM and D0 collaborations. We then describe the gap between jet measurements sensitive to the high gluon density regime and the possible observation of the saturation phenomenon in PbPb interactions. We also mention the sensitivity to beyond the Standard Model physics and to the production of axion-like particles via photon–photon interactions.

DOI:10.5506/APhysPolB.57.6-A10

1. Introduction

In this paper, we present some recent results on Quantum Chromodynamics (QCD) diffraction at the LHC, mainly from the CMS and TOTEM experiments. We start by presenting the discovery of the odderon by comparing the elastic cross section measurements in pp and $p\bar{p}$ interactions by the TOTEM and D0 collaborations at the LHC and the Tevatron. We then discuss the possible observation of the high gluonic density regime at the LHC, and especially of the saturation phenomenon in heavy-ion interactions such as PbPb. We finish this report by discussing the sensitivity to beyond the Standard Model physics and the production of axion-like particles considering the LHC as a $\gamma\gamma$ collider.

These studies originate from a long-term collaboration with Prof. Andrzej Białas and Prof. Robi Peschanski that started after my Ph.D. in Saclay about the dipole model and diffraction [1] and I would like to express all my gratitude to Andrzej and Robi for this long-term and successful collaboration. I wish Andrzej a very nice birthday.

* Funded by SCOAP[3] under Creative Commons License, CC-BY 4.0.

2. The discovery of the odderon

The comparison of the elastic event measurements at the LHC and the Tevatron, respectively in pp and $p\bar{p}$ collisions, led recently to the discovery of the odderon [2]. In elastic interactions, each proton or antiproton remains intact after interaction and is scattered at some angles, and can lose or gain some momentum. Nothing is produced in addition to the intact proton or antiproton. Measuring elastic collisions thus requires the detection of intact protons or antiprotons after the collision, using dedicated detectors called Roman Pots. These detectors can move very close to the beam (up to 3σ at the LHC, for instance) when beams are stable, so that protons scattered at very small angles can be measured. The TOTEM [3] and ATLAS/ALFA [4] collaborations installed Roman Pots at about 220 m from the interaction point, and the D0 Collaboration had similar detectors at about 23 and 31 m [5]. Just before the end of the Tevatron, the D0 Collaboration measured the elastic $p\bar{p}$ $\mathrm{d}\sigma/\mathrm{d}t$ cross section at a center-of-mass energy $\sqrt{s}$ of 1.96 TeV for $0.26 < |t| < 1.2$ GeV^2, where t is the square of the four-momentum transferred at the proton/antiproton vertex measured by tracking the proton/antiproton [6]. D0 data are displayed in Fig. 1. The TOTEM Collaboration measured the elastic pp $\mathrm{d}\sigma/\mathrm{d}t$ at $\sqrt{s} = 2.76$, 7, 8, and 13 TeV [7] as shown in Fig. 2. The advantage of the TOTEM detector is that it includes very forward telescope covering rapidity regions $3.1 < |\eta| < 4.7$ (telescope T1) and $5.3 < |\eta| < 6.5$ (telescope T2), allowing to veto any additional particles emitted in the very forward region for elastic interactions.

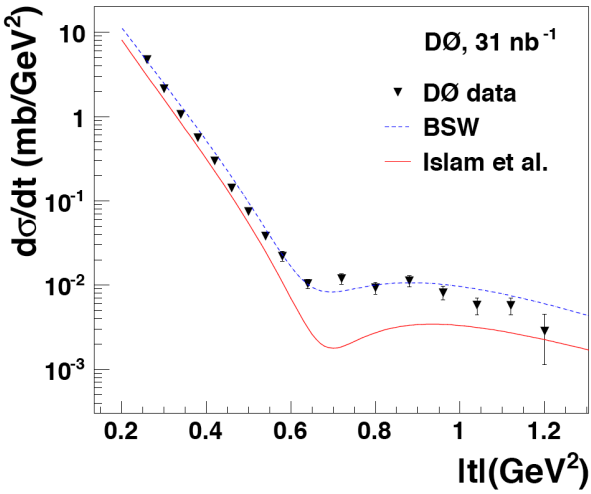

Fig. 1. $p\bar{p}$ elastic $\mathrm{d}\sigma/\mathrm{d}t$ cross section as a function of $|t|$ measured by the D0 Collaboration at 1.96 TeV.

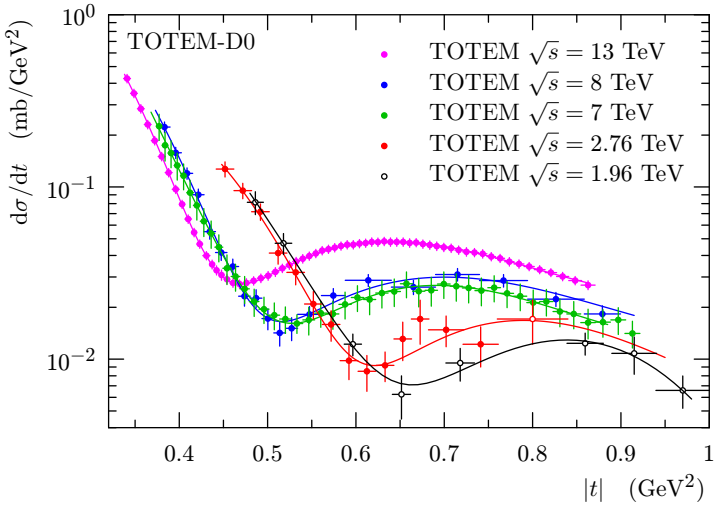

Fig. 2. pp elastic $d\sigma/dt$ cross section as a function of $|t|$ measured by the TOTEM Collaboration at 2.76, 7, 8, and 13 TeV, and extrapolated down to 1.96 TeV in black.

Elastic scattering can be explained by the exchange of colorless objects, Pomeron and odderon, that correspond to positive and negative charge parity C [8–11]. The odderon is defined as a singularity in the complex plane of the t-channel partial wave J, located at $J = 1$, when $t = 0$, and which contributes to the odd crossing amplitude. The QCD treatment of the odderon was performed considering multi-gluon exchanges in hadron–hadron interactions in elastic pp interactions [12]. In QCD, the Pomeron is made of an even number of gluons leading to a $(+1)$ C-parity, whereas the odderon is made of an odd number of gluons corresponding to a (-1) C-parity. The elastic scattering amplitudes for pp and $p\bar{p}$ interactions can be written as the sum or the difference of the even and the odd parts of the amplitude

$$\begin{aligned} A_{pp} &= \text{Even} + \text{Odd}\,, \\ A_{p\bar{p}} &= \text{Even} - \text{Odd}\,. \end{aligned} \tag{1}$$

From these equations, it is clear that observing a difference between pp and $p\bar{p}$ interactions would be a clear way to observe the odderon. Our idea was thus to obtain a quantitative measurement of the differences between elastic pp and $\bar{p}p$ cross sections.

Let us note that there was already some indication of possible differences at the ISR energies between pp and $p\bar{p}$ interactions [13], but this was not considered to be a proof of the existence of the odderon due to possible additional reggeon and meson exchanges at lower $\sqrt{s}$. At high energies

of the order of 1 TeV or higher, the contribution of Reggeon and meson exchanges becomes negligible, and a potential difference between pp and $p\bar{p}$ elastic cross section is solely due to the odderon.

As seen in Figs. 1 and 2, elastic $\mathrm{d}\sigma/\mathrm{d}t$ cross sections show different behaviors between pp and $p\bar{p}$ interactions. There is a maximum (the bump) and a minimum (the dip) for pp interactions at all $\sqrt{s}$, whereas such behavior is not observed in $p\bar{p}$ interactions. In order to compare directly elastic pp and $p\bar{p}$ cross sections, one needs to extrapolate the TOTEM measurements at 2.76, 7, 8, and 12 TeV down to 1.96 TeV, *i.e.* to the Tevatron $\sqrt{s}$. Unfortunately, a direct comparison is not possible since there is no acceptance for the TOTEM Roman Pots at 1.96 TeV, in the dip and bump regions, where we perform the comparison. We define a series of eight points in the $\mathrm{d}\sigma/\mathrm{d}t$ cross section (we give both the t and $\mathrm{d}\sigma/\mathrm{d}t$ values) that are characteristic of the elastic pp cross-section shape as shown in Fig. 3, namely the *bump*, *dip*, *dip2*, and *bump2* corresponding to the same cross section as the dip and the bump but at lower $|t|$, *mid1* and *mid2* in the middle of the cross section between the dip and the bump, and finally *bump+5* and *bump+10* that correspond to the cross sections 5 and 10 times the difference between the bump and the dip.

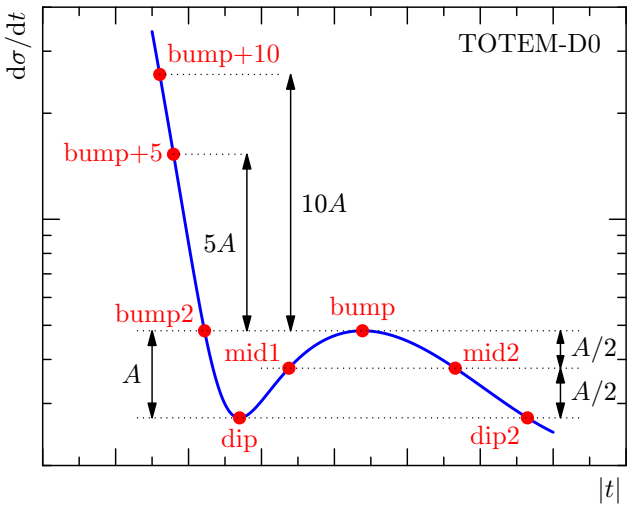

Fig. 3. Definition of the points that are characteristic of the shape of elastic pp cross sections (see the text).

The bump over dip ratio measured for pp and $p\bar{p}$ elastic interactions at the ISR [13], Tevatron, and LHC energies is shown in Fig. 4. In pp elastic collisions, it decreases as a function of $\sqrt{s}$ up to $\sim$ 100 GeV and is flat above. D0 $p\bar{p}$ shows a ratio of 1.00 ± 0.21 given the fact that neither bump

nor dip is observed in $p\bar{p}$ data within uncertainties. It leads to a more than 3σ difference between pp and $p\bar{p}$ elastic data (assuming a flat behavior above $\sqrt{s} = 100$ GeV).

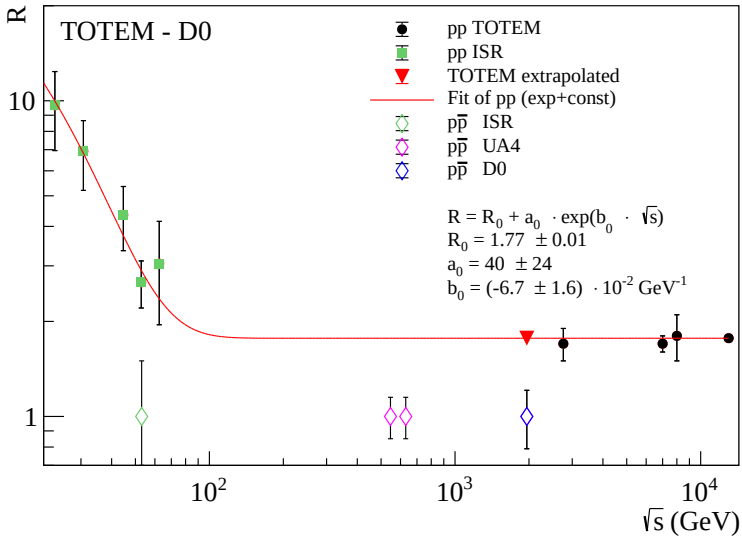

Fig. 4. Bump over dip ratio for pp and $p\bar{p}$ elastic cross sections.

An even more quantitative comparison is possible using the eight characteristic points described above. The values of $|t|$ and $\mathrm{d}\sigma/\mathrm{d}t$ for these eight points are shown in Fig. 5 as a function of $\sqrt{s}$ of 2.76, 7, 8, and 13 TeV extrapolated down to the Tevatron $\sqrt{s} = 1.96$ TeV, using a two-parameter fit

$$|t| = a \log\left(\sqrt{s}\ [\mathrm{TeV}]\right) + b\,, \tag{2}$$

$$(\mathrm{d}\sigma/\mathrm{d}t) = c\sqrt{s}\ [\mathrm{TeV}] + d\,. \tag{3}$$

Note that the extrapolation at 1.96 TeV using a variety of different fitting functions is well within uncertainties.

Using the extrapolated characteristic points from the TOTEM measurements, it is now possible to predict the elastic pp cross sections at the Tevatron energies in the same $|t|$ bins as for the D0 measurement. Differences in normalization are taken into account by adjusting the TOTEM and D0 data sets to have the same cross sections at the optical point (OP) $\mathrm{d}\sigma/\mathrm{d}t(t = 0)$ (OP cross sections are expected to be equal if there are only C-even exchanges). We first predict the pp total cross section from an extrapolated fit to the TOTEM data with a $\chi^2 = 0.27$

$$\sigma_{\mathrm{tot}} = a_2 \log^2 \sqrt{s}\ [\mathrm{TeV}] + b_2\,, \tag{4}$$

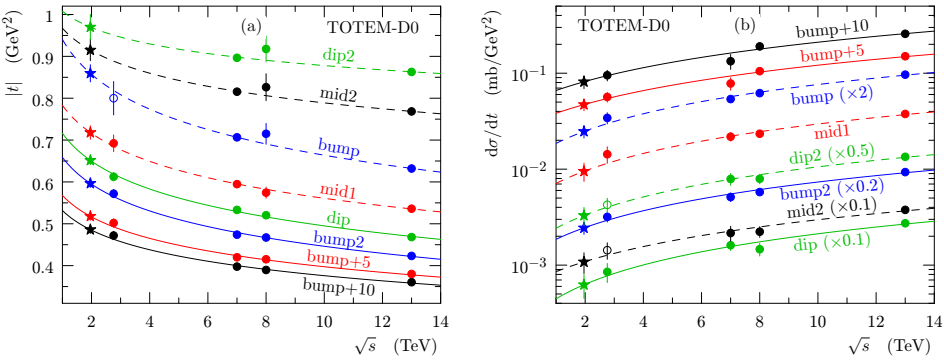

Fig. 5. Variation of the t and $\mathrm{d}\sigma/\mathrm{d}t$ values for the reference points at $\sqrt{s} = 2.76$, 7, 8, and 13 TeV extrapolated down to the Tevatron energies $\sqrt{s} = 1.96$ TeV (stars).

that leads to an estimate of pp $\sigma_{\mathrm{tot}} = 82.7 \pm 3.1$ mb at 1.96 TeV. Different parametrizations (for instance, a 3-parameter formula including a $\log s$ term) lead to similar results within uncertainties. From the extrapolated TOTEM pp σ_{tot} at 1.96 TeV, it is possible to extract $\mathrm{d}\sigma/\mathrm{d}t(t = 0)$ using

$$\sigma_{\mathrm{tot}} = \sqrt{\frac{16\pi(\hbar c)^2}{1+\rho^2} \left.\frac{\mathrm{d}\sigma}{\mathrm{d}t}\right|_{t=0}}. \tag{5}$$

Assuming the ratio of the imaginary and real parts of the elastic amplitude is $\rho = 0.145$, as taken from COMPETE [14], this leads to $\mathrm{d}\sigma/\mathrm{d}t(t = 0)$ at the OP of 357.1 ± 26.4 mb/GeV^2 from the TOTEM data (since the dependence on ρ is squared in Eq. (5), the result does not depend strongly on the exact value of ρ). The D0 Collaboration measured the optical point of $\mathrm{d}\sigma/\mathrm{d}t$ at small t to be 341 ± 48 mb/GeV^2, and we thus rescale the TOTEM data by the ratio 0.954 ± 0.071, which is compatible with 1.0 within uncertainties. Please note that we do not claim that we performed a measurement of $\mathrm{d}\sigma/\mathrm{d}t$ at the OP at $t = 0$ (it would require additional measurements closer to $t = 0$), but we use the two extrapolations in order to obtain a common and somewhat arbitrary normalization point.

The comparison between the D0 $p\bar{p}$ elastic cross-section measurements and the extrapolated TOTEM pp elastic data down to the Tevatron energies is shown in Fig. 6. The χ^2 test with six degrees of freedom yields a p-value of 0.00061, corresponding to a significance of 3.4σ. This result can be combined with the independent evidence of the odderon found by TOTEM using the ρ and total cross-section measurements at low t [15] which leads to a 5.3 to 5.7σ discovery [2] depending on the models [14] for ρ.

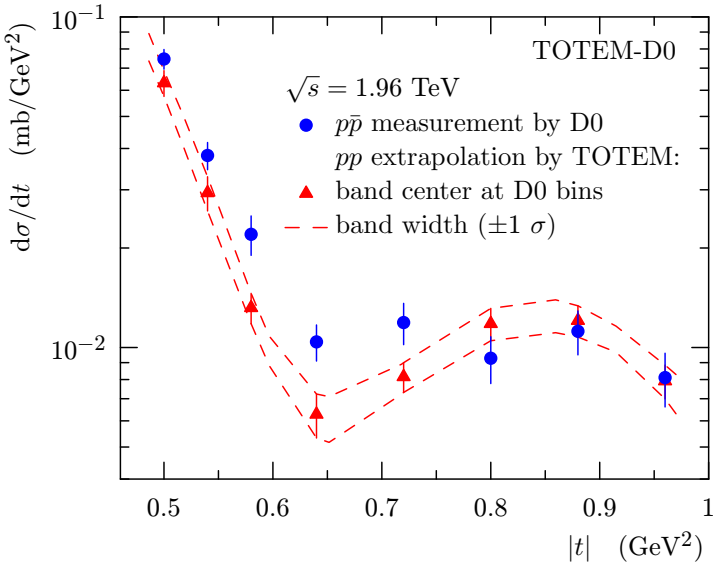

Fig. 6. Comparison between the elastic $d\sigma/dt$ cross-section measurements at $\sqrt{s} = 1.96$ TeV by the D0 Collaboration for $p\bar{p}$ interactions and by the TOTEM Collaboration for pp interactions, extrapolated from measurements at 2.76, 7, 8, and 13 TeV. The difference can be explained by the existence of the odderon.

3. A new scaling in elastic data

In this section, we will discuss a new scaling that appears in elastic $d\sigma/dt$ cross sections [16, 17]. The fact that we can use the same fitting formulae (see Eqs. (2) and (3)) to describe the evolution of all characteristic points as a function of $\sqrt{s}$ shows that all $d\sigma/dt$ cross sections for $\sqrt{s} = 2.76$, 7, 8, and 13 TeV are stackable with each other as suggested in Fig. 2.

In order to introduce a new scaling in elastic data, we first introduce the variable $t^* = (s/|t|)^A \times |t|$, inspired by geometric scaling in terms of saturation models [18], and $t^{**} = t^*/s^B$, A and B being parameters to be fitted to data [16]. In fact, A and B are correlated, and we have a full valley of parameters leading to similar scalings ($B = A - 0.065$), that leads to one single-parameter fit to data ($A = 0.28$). As shown in Fig. 7, $d\sigma/dt^*$ shows scaling as a function of t^{**}. The s dependence on $d\sigma/dt$ is imposed by scaling as $s^{-\alpha}$, where $\alpha = -A(A-1.065)/(1-A) = 0.305$. Scaling is not supposed to work perfectly at low $|t|$ that corresponds to the QED Coulomb and non-perturbative QCD region, and at high $|t|$ in the perturbative QCD domain.

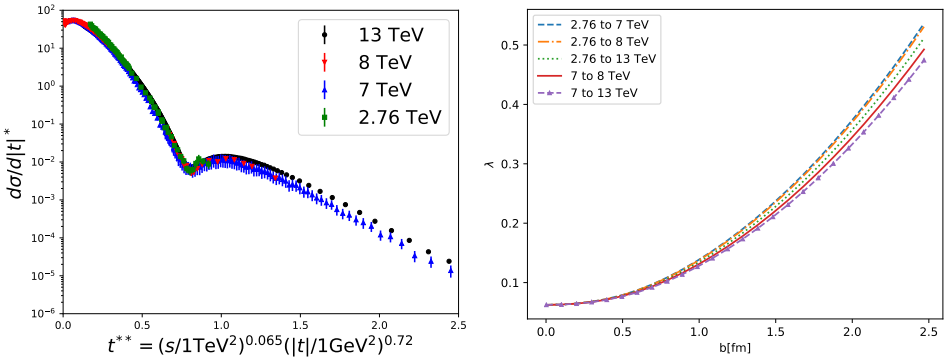

Fig. 7. Left: $\mathrm{d}\sigma/\mathrm{d}t^*$ as a function of $t^{**} = t^*/s^{0.215}$, where $t^* = (s/|t|)^{0.28} \times |t|$ showing a scaling in elastic $\mathrm{d}\sigma/\mathrm{d}t$ cross sections measured by the TOTEM Collaboration at 2.76, 7, 8, and 13 TeV. Right: Power growth exponent λ as a function of b for various reference $\sqrt{s}$ pairs.

The next step is to compute the profile function Γ in the impact parameter space. We first perform a fit of the elastic amplitude A using the definition

$$\frac{\mathrm{d}\sigma}{\mathrm{d}|t|} = \frac{1}{16\pi s^2}|A(s,t)|^2 = |\mathcal{A}(s,t)|^2 \,. \tag{6}$$

The fit formula is the following:

$$\mathcal{A}(s,t) \;=\; i\left(\mathcal{A}_1(s,t) + \mathcal{A}_2(s,t)\right)\; \mathrm{e}^{i\theta} \,, \tag{7}$$

$$\mathcal{A}_1(s,t) \;=\; N_1(s)\,\mathrm{e}^{-B_1(s)|t|} \,, \tag{8}$$

$$\mathcal{A}_2(s,t) \;=\; N_2(s)\,\mathrm{e}^{-B_2(s)|t|}\,\mathrm{e}^{i\phi} \,, \tag{9}$$

where $N_1(s) = N_1^0 s^{\alpha/2}$, $N_2(s) = N_2^0 s^{\alpha/2}$, $B_1(s) = B_1^0 s^{\gamma/2}$, and $B_2(s) = B_2^0 s^{\gamma/2}$. There are six free parameters in the fit, namely N_1^0, N_2^0, B_1^0, B_2^0, ϕ, and θ. $\alpha = 0.305$ and $\gamma/2 \equiv 0.065/(1-A) = 0.065/0.72 \approx 0.09$ being fixed by scaling. The fit quality is quite good with a $\chi^2/\mathrm{d.o.f.} = 1.08$ for $0.2 < t^{**} < 1.5$ in the dip–bump region for 476 data points. We then compute the profile function Γ in the impact b-parameter space using the following equation:

$$\mathrm{Re}\left(\Gamma(s,b)\right) = \frac{1}{4\pi i s}\int_0^\infty \mathrm{d}q\, q\, J_0(qb)\, A\left(s, t=-q^2\right) \,, \tag{10}$$

where J_0 is the 0^{th} order Bessel function.

We define λ as a function of the ratio of two values of Γ for two values of $\sqrt{s}$ as

$$\lambda = \frac{1}{\ln(s_1/s_2)} \ln\left(\frac{\mathrm{Re}\,\Gamma(s_1,b)}{\mathrm{Re}\,\Gamma(s_2,b)}\right) \,. \tag{11}$$

The values of λ as a function of b for different $\sqrt{s}$ are shown in Fig. 7, right. $\lambda = (\alpha - \gamma)/2 = 0.06$ when $b \to 0$ as predicted by scaling. This means that scaling predicts a universal behavior of λ at small b. Values of λ at small b are compatible with expectations from a dense object, such as a black disc, and reach higher values around 0.3 for $b = 1$ fm, which recalls the power-law exponent in the small-x limit of QCD, described by the perturbative Balitsky, Fadin, Kuraev, Lipatov (BFKL) evolution equation [19] at next-to-leading logarithmic accuracy. In this sense, we can interpret our results as the presence of dense gluonic objects in the proton at high energy. The density of these objects in the proton can be small, but the density of the gluons inside can be large.

A similar scaling was described in Ref. [17]. The bump over dip elastic cross-section $\mathrm{d}\sigma/\mathrm{d}t$ ratio is constant at high energies, and the position ratio in $|t|$ between the bump and the dip is also constant between the ISR and LHC energies. This leads to a new scaling of $W^{-\alpha}\frac{\mathrm{d}\sigma_{\mathrm{el}}}{\mathrm{d}t}(\tau)$ as a function of $\tau = W^{\beta}|t|$ with $\alpha = 0.66$ (with large uncertianties) and $\beta = 0.1686$.

4. High gluon density regime at the LHC

In this section, we describe new observables that are sensitive to the high gluon density regime at the LHC. We consider two evolution equations to describe the structure of protons or heavy ions, namely the Dokshitzer, Gribov, Lipatov, Altarelli, Parisi (DGLAP) [20] evolution in resolution Q^2 (resumming terms in $\alpha_{\mathrm{s}} \log Q^2$, resolving "smaller" partons at high Q) and the BFKL [19] evolution in energy x (resumming terms in $\alpha_{\mathrm{s}} \log 1/x$ leading to large parton densities at small x). Ultimately, at very small x, the domain of saturation or gluon recombination can be reached, that leads to slower evolution of gluon densities as a function of energy.

Many observables have been suggested to look for the high gluon density regime at small x such as the measurement of a large interval in rapidity between jets, the so-called Mueller–Navelet jets [21–23], the measurement of the azimuthal angle between jets [24], or the measurement of the gap between jets [25, 26]. We will focus on this last measurement performed by the CMS Collaboration, namely the cross section of two jets separated by a large interval in rapidity, where the region $(-1 < \eta < 1)$ is devoid of any charged particle production (requesting the absence of reconstructed tracks with a transverse momentum above 200 MeV) [25]. Requesting a gap between the two jets is only possible using special runs at the LHC with small pile-up.

The cross section predicted by NLO DGLAP is expected to be negligible for large gaps, below what can be measured, and is thus a clean test of the BFKL resummation. In Fig. 8, we display the fraction of the gap

between jet events as a function of the transverse momentum of the second leading jet, the difference in rapidity and in azimuthal angle between the two jets. Data are compared to different models [26]. We will only discuss two of them, namely the experimental gap (in dashed red line) and the strict gap definition (in dark green full line), assuming the BFKL evolution equation [19]. The first model corresponds to the experimental definition of the

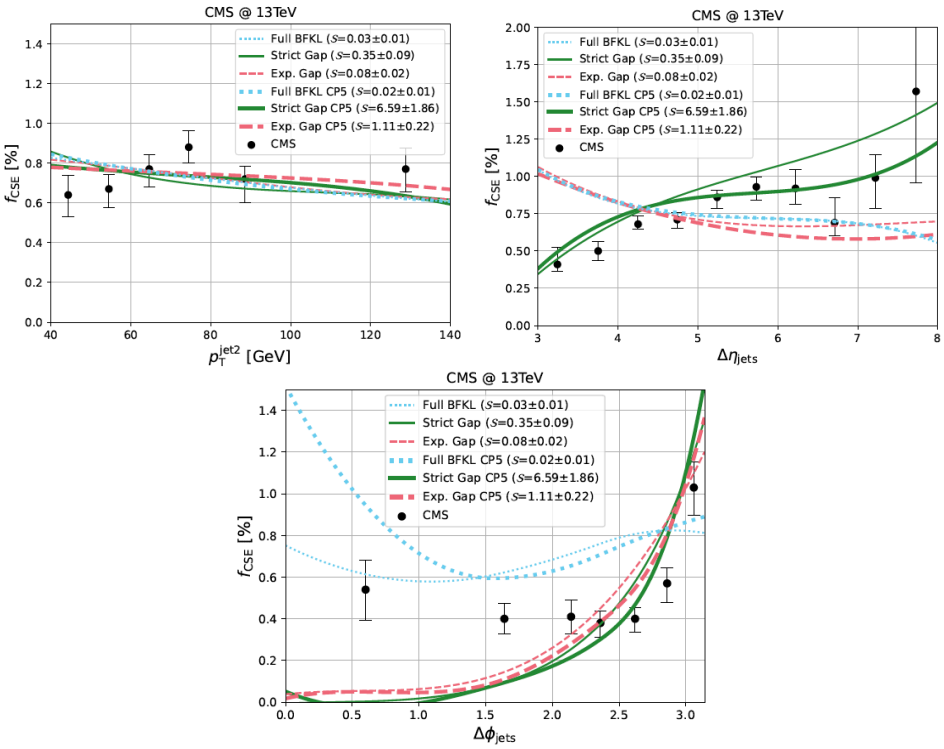

Fig. 8. Fraction of the gap between jet events as a function of the transverse momentum of the second leading jet, the interval in rapidity and in azimuthal angle between the two jets, compared to different models.

gap as performed by the CMS Collaboration, namely the absence of charged particles above 200 MeV in the gap region ($-1 < \eta < 1$). It leads to a bad description of data especially for the difference in rapidity between the two jets. The second model corresponding to a strict gap definition (no particle above 1 MeV in the gap region) leads to a good description of data except at very low $\Delta\phi$. It is, of course, not possible to achieve this threshold experimentally. However, to understand why it leads to a fair description of data, we noticed that the distribution of charged particles from PYTHIA 8 [27] in the gap region ($-1 < \eta < 1$) with the initial-state radiation is very large.

Particles emitted at large angle with $p_{\mathrm{T}} > 200$ MeV from the initial-state radiation have a large influence on the presence or absence of a gap, and thus, on the gap definition (experimental or strict). Retuning the amount of initial-state radiation allows for obtaining a good agreement for the ratio of the gap between jet events using the experimental gap definition [26].

We also computed a full calculation of the jet–gap–jet cross section at next-to-leading logarithm accuracy, using the next-to-leading orders BFKL kernel and impact factors [28]. Compared to the results obtained with leading order impact factors, the effect is quite small leading to a higher cross section by about 20% at high jet p_{T}, and shows even a smaller effect on the rapidity dependence. The total uncertainties due to the scale variation are also smaller, of the order of 15–20%.

The CMS Collaboration measured the subsample of the gap between jet events requesting in addition at least one intact proton on either side of the CMS in the TOTEM Roman Pot detectors [25]. Eleven events were observed with a gap between jets of $(-1 < \eta < 1)$ and at least one proton tagged with ~ 0.7 pb^{-1}, as shown in Fig. 9. Jet–gap–jet events were observed for the first time by the CMS Collaboration. This leads to very clean events for jet–gap–jets measurements since the effects of multi-parton interactions are suppressed. This might be the ideal way to probe low-x (BFKL) resummation effects [29] and would benefit from more statistics (about 10 pb^{-1} for single diffractive and 100 pb^{-1} for double Pomeron exchange events of low pile-up data would be needed to perform some measurements of differential distributions).

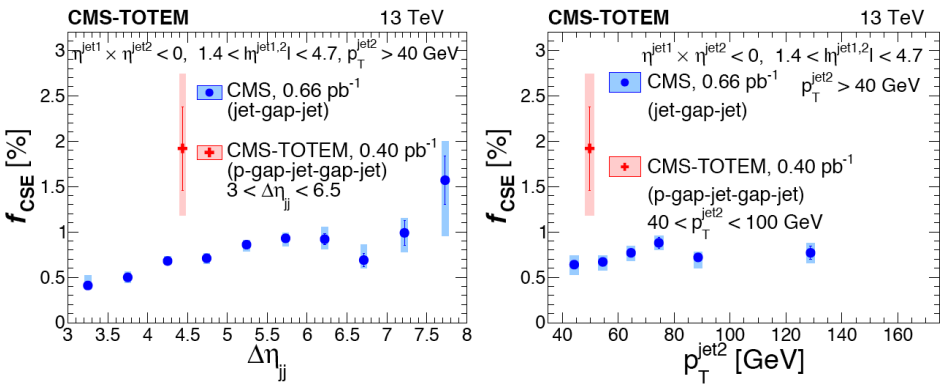

Fig. 9. Fraction of the gap between jet events as a function of the interval in rapidity between the two jets and the transverse momentum of the second leading jet for inclusive (blue points) and diffractive (red points) events when a proton is detected in the TOTEM Roman Pots. Eleven events were observed with 0.7 pb^{-1}.

Using the measurement of the gap between jets at the LHC, we now have some evidence of the BFKL resummation of the high gluon density regime at the LHC and we can study if we can reach the domain of saturation.

5. Possible observation of saturation phenomenon in PbPb collisions at the LHC

In this section, we will discuss the possible observation of the saturation phenomenon at the LHC. When the value of x becomes small, the number of gluons in the proton (or heavy ions) becomes very large. The usual linear equations of QCD (DGLAP or BFKL) are no longer valid, and one needs to consider recombination of gluons leading to non-linear evolution equations such as the Balitsky–Kovchegov (BK) [30] equation. This leads to the saturation phenomenon or slower evolution of the energy dependence of the gluon density. The idea is to look for the best observables sensitive to saturation in PbPb interactions.

5.1. Exclusive vector meson production

A scheme of the sensitivity to saturation for vector meson production is shown in Fig. 10, left. In order to see saturation effects, one needs to have a dense object with a high gluon content, such as Pb. In addition, we need a characteristic scale (for instance, the mass of the vector meson), which is above the perturbative scale (of the order of 1 GeV) to trust the perturbative calculation and below the saturation scale Q_S. Q_S is of the order of 1 GeV for protons, whereas it is increased by $A^{1/3}$ for heavy ions ($Q_S \sim 5.8$ GeV for Pb). Exclusive J/Ψ production with a scale squared $m^2_{J/\Psi} \sim 10$ GeV^2 is ideal to observe saturation being below Q_S^2. On the contrary, the exclusive production of the Υ meson should not be showing much saturation effects since its scale $M^2_\Upsilon \sim 100$ GeV^2 is above Q_S^2. The exclusive production of ρ mesons has a scale $m^2_\rho \sim 1$ GeV^2 well below Q_S^2, but of the same order of magnitude as the lower limit of the perturbative scale, which makes it difficult to rely on perturbative calculations. The diagram showing vector meson production in γA interactions (the γ being emitted by the Pb ion) for diffractive events, where A is intact after the collision, is shown in Fig. 10, right. In the case of inclusive production, the two-gluon exchange should be replaced by a single one. Using the vector meson production, one probes the gluon content of A which could be a proton (resp. Pb) in the case of pPb (resp. PbPb) interactions. Saturation effects are expected, for instance, in

the J/Ψ exclusive production, when one probes the gluon content in Pb ($m^2_{J/\Psi} < Q^2_{\rm S} \sim 34$ GeV^2) but not for protons ($m^2_{J/\Psi} > Q^2_{\rm S} = 1$ GeV^2). We have a similar situation when we consider the exclusive production of $c\bar{c}$ and $b\bar{b}$, where the typical scale can be below $Q_{\rm S}$ in γPb interactions.

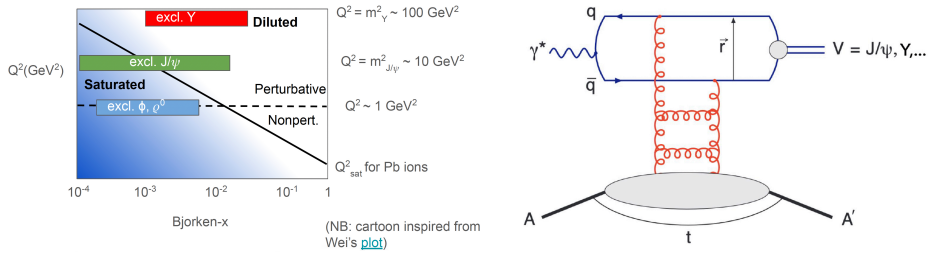

Fig. 10. Left: Scheme of sensitivity to saturation for vector meson production. Right: Exclusive vector meson production in γPb interactions.

To compute the exclusive production of J/Ψ or Υ, the process can be factorized in two parts, namely the photon fluctuation into a quark–antiquark pair, and the quark–antiquark pair interacting with the target hadron. The first part is described by the light-cone wave function of the photon computed using QED and the second part of the process is given by the dipole scattering amplitude which is non-perturbative. However, its energy dependence can be described using a perturbative evolution equation with and without saturation effects using the BK [30] or the BFKL [19] equations. The dipole amplitude at the starting scale of the evolution is fixed by fitting the predictions to measured data, for instance, the cross section of vector meson production at HERA [31]. We also take into account b impact parameter dependence in the dipole amplitude. We modify the traditional McLerran–Venugopalan model by taking the b dependence with a Gaussian form of the thickness function [32]

$$T(b) = \frac{1}{2\pi B_P} \, {\rm e}^{-b^2/(2B_P)} \, . \tag{12}$$

There is a large difference between taking into account or not the b impact parameter dependence for γp cross sections, and the effect is smaller for γPb interactions since a nucleus is much larger than a proton and neglecting impact parameter dependence is more justified [32]. Technically, we will study the effect of saturation in the following by comparing the evolution of cross sections as a function of energy W using either the BK or the BFKL equations (which is equivalent to neglecting the gluon recombination term in BK) including running $\alpha_{\rm s}$.

In Fig. 11, we display the exclusive J/Ψ production cross section as a function of the center-of-mass energy W for γp (left), γPb (center) interactions, and the nuclear suppression factor (right) from the H1 [33] and ZEUS [34] collaborations at HERA and the ALICE [36], CMS [35], and LHCb [37] collaborations at the LHC, compared to predictions with and without saturation [31]. For the J/Ψ production in γp interactions, small differences are observed between the BK and BFKL evolution and there is no sign for saturation as expected, since one probes the gluon in the proton. On the contrary, γPb cross sections clearly favor saturation models. The difference between the BFKL and BFKL-adjusted predictions corresponds to a small variation in $\Lambda_{\rm QCD}$ to obtain a better description of data in γp interactions. It seems that data even show more saturation effects than our calculation but it is worth noting that an impact parameter NLO BK equation would be needed in order to compute more precise predictions for γPb interactions. Our goal was more to show that the linear BFKL evolution equation seems to be disfavored and some additional effect such as saturation is needed to describe data. However, alternative approaches such as nuclear PDFs including shadowing can also lead to a good description of the J/Ψ exclusive cross sections, and we will propose an additional measurement to distinguish between both models in the following subsection.

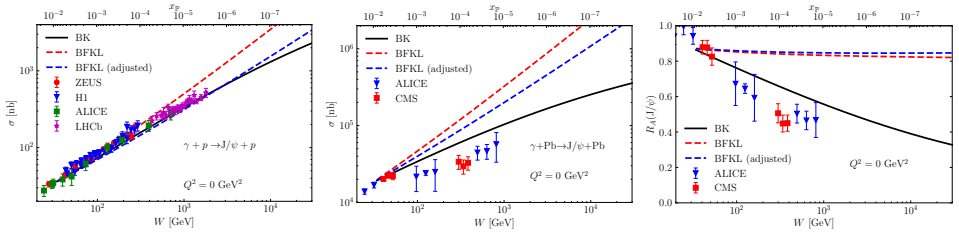

Fig. 11. Exclusive J/Ψ production cross section as a function of the center-of-mass energy W. Left: γp, center: γPb, right: nuclear suppression factor. Predictions without (BFKL) and with saturation (BK) are compared with measurements at HERA (H1 and ZEUS) and at the LHC (ALICE, CMS and LHCb).

In Fig. 12, we display similar results for the exclusive Υ production as a function of W for γp (left), γPb (center) interactions, and the nuclear suppression factor (right). As expected, there is a good agreement between the BK and BFKL predictions and data for γp cross sections and small differences are observed between both approaches. In γPb interactions, small differences are also predicted between the BK and BFKL evolutions for $W \sim 1$ TeV because of the Υ vector meson mass. Recent measurements from the CMS Collaboration are compatible with this prediction [38].

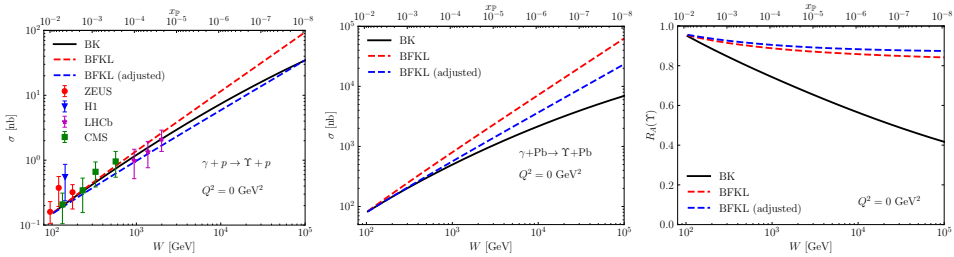

Fig. 12. Exclusive Υ production cross section as a function of the center-of-mass energy W. Left: γp, center: γPb, right: Nuclear suppression factor. Predictions without (BFKL) and with saturation (BK) are compared with measurements at HERA (H1 and ZEUS) and at the LHC (CMS and LHCb).

5.2. $c\bar{c}$ and $b\bar{b}$ production

In this subsection, we discuss additional possible measurements that are sensitive to saturation effects and that might allow one to distinguish between color glass condensate (saturation), and nuclear PDFs and shadowing approaches [39]. We consider the production of $c\bar{c}$ (in red) and $b\bar{b}$ (in blue) in γp and γPb interactions, respectively, in Figs. 13 and 14 using the BFKL (dashed line) and the BK (full line) evolution. The left figure corresponds to the inclusive cross section (when one gluon is exchanged with the proton or with Pb), whereas the right one to the diffractive one when the proton or Pb is intact after the interaction. As expected, not much difference is observed for γp interactions between the BFKL and BK evolution, whereas a difference of about a factor of two is observed for γPb interactions for diffractive production at $W \sim 1$ TeV.

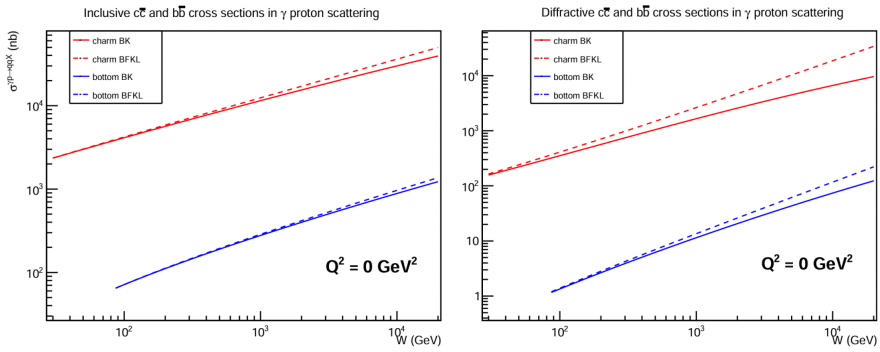

Fig. 13. Inclusive (left) and diffractive (right) $c\bar{c}$ (in red) and $b\bar{b}$ (in blue) production cross sections for γp interactions. The BFKL predictions are in dashed lines and the BK ones including saturation effects in full line.

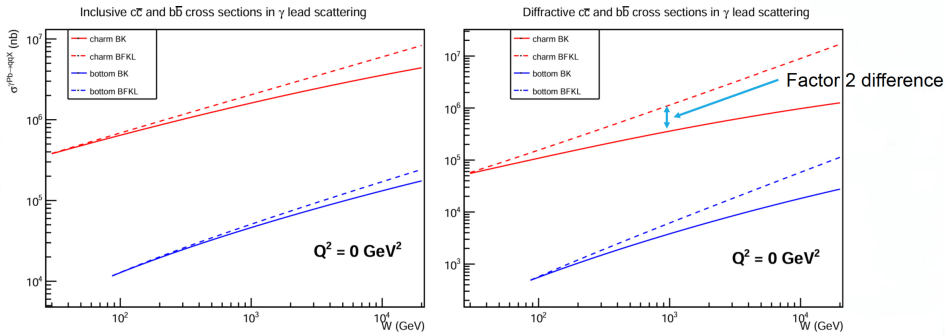

Fig. 14. Inclusive (left) and diffractive (right) $c\bar{c}$ (in red) and $b\bar{b}$ (in blue) production cross sections for γPb interactions. The BFKL predictions are in dashed lines and the BK ones including saturation effects in full line.

The ratio of the diffractive to the inclusive $c\bar{c}$ production cross sections as predicted by the BK evolution for γp (left) and γPb (right) interactions is shown in Fig. 15. In the case of protons, we predict a ratio of about 12% which is compatible with what was observed at HERA, and in the case of Pb, we predict a ratio of about 21%. CMS accumulated PbPb interaction data in 2025 that will allow for this measurement to be performed (for previous data taking, a positive signal in the zero-degree calorimeter was requested at trigger level, removing the diffractive events when Pb is intact after interaction). Such a high percentage of diffractive events will be a clean test of the CGC-like models and will probably allow one to distinguish it from the nuclear PDFs and shadowing approaches which predict a lower fraction of diffractive events.

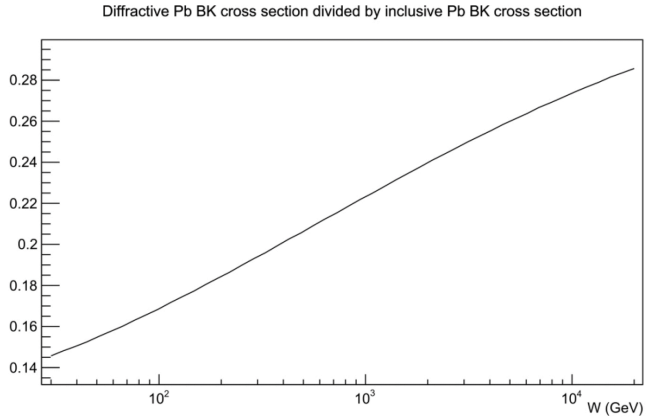

Fig. 15. Ratio of the diffractive to the inclusive $c\bar{c}$ production cross sections as predicted by the BK evolution for γp (left) and γPb (right) interactions.

Measuring UPC vector meson and charm/beauty production at the LHC and the EIC for different ion interactions will thus be fundamental to probe saturation models. The reached kinematical domain is complementary between the LHC and the EIC allowing to obtain measurements with unprecedented precision over a wide domain in energy. The feasibility of running both machines with different ions (He, O, Ar, Ne, Pb, *etc.*) will allow one to study the path towards the saturation regime, which will appear for heavier ions but not for the light ones, while measuring the nuclear PDFs with high precision.

6. $\gamma\gamma$ physics at the LHC

In this section, we will describe the reach in beyond the Standard Model physics (especially the production of axion-like particles) when one considers the LHC as a $\gamma\gamma$ collider. The diagrams for exclusive productions via gluon or photon exchanges are shown in Fig. 16. The QCD diagram dominates at low diffractive masses (dijet masses, for instance) up to masses of about 120 GeV. This allows one to study the exclusive production of low mass particles such as pion pair or glueballs in a very clean environment (one can produce glueballs that decay into $\rho\rho$, $\phi\phi$, K^*K^*, $\omega\omega$, for instance), in addition to more standard studies of Pomeron structure in terms of quarks and gluons using diffractive production of jets, photon and jet, W asymmetries, *etc.* [40]. In this section, we will focus on the exclusive production of γ, W, Z pairs at high masses which is dominated by photon exchanges. We thus consider the LHC as a $\gamma\gamma$ collider. Most of the results in this section assume that we measure the intact protons after collision in the Precision Proton Spectrometer (PPS) [41] by the CMS and TOTEM collaborations or the ATLAS Forward Proton (AFP) by the ATLAS Collaboration [42], that leads to a good acceptance in diffractive mass above about 450 GeV.

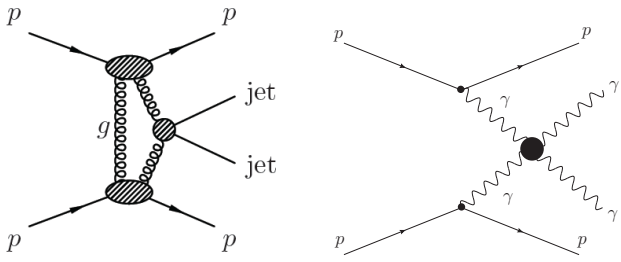

Fig. 16. Exclusive dijet production via gluon exchanges (QCD process) processes (left) and of diphotons via photon exchanges (QED process, right).

In Fig. 16, right, we display the diagram of exclusive $\gamma\gamma$ via photon exchanges. Similar diagrams also include the production of WW, ZZ, $t\bar{t}$, and γZ. As an example, the SM exclusive production of WW is $\sigma_{WW} = 95.6$ fb, and $\sigma_{WW}(W = M_X > 1 \text{ TeV}) = 5.9$ fb, which shows that many events will be produced at high mass at the LHC (the typical luminosity for Run 3 is 300 fb^{-1} and will increase to 3000 fb^{-1} at the high-luminosity LHC). The exclusive production of WW, ZZ, $\gamma\gamma$, $t\bar{t}$, γZ will thus be sensitive to different quartic anomalous couplings involving photons, and represents a stringent test of QED [43, 44].

We will first consider the exclusive $\gamma\gamma$ production via photon exchanges as an example. The SM cross section for such a process for diphoton masses above 450 GeV (in the PPS acceptance) is very small and leads to a negligible number of events. Anomalous quartic $\gamma\gamma\gamma\gamma$ can appear via loops of new particles or resonances decaying into two photons such as axion-like particles (ALPs). We introduce two effective operators at low energies in the Lagrangian due to quartic anomalous couplings

$$L_{4\gamma} = \zeta_1^{\gamma} F_{\mu\nu} F^{\mu\nu} F_{\rho\sigma} F^{\rho\sigma} + \zeta_2^{\gamma} F_{\mu\nu} F^{\nu\rho} F_{\rho\lambda} F^{\lambda\mu} \,, \tag{13}$$

and $\gamma\gamma\gamma\gamma$ couplings can be modified in a model-independent way by loops of heavy charged particles

$$\zeta_1 = \alpha_{\text{em}}^2 Q^4 m^{-4} N c_{1,s} \,, \tag{14}$$

where the coupling depends only on $Q^4 m^{-4}$ (charge and mass of the charged particle) and on spin, $c_{1,s}$ which leads to ζ_1 of the order of 10^{-14}–10^{-13} GeV^{-4}. ζ_1 can also be modified by neutral particles at tree level (extensions of the SM including scalar, pseudo-scalar, and spin-2 resonances that couple to the photon)

$$\zeta_1 = (f_{\text{S}} m)^{-2} d_{1,s} \,, \tag{15}$$

where f_{S} is the $\gamma\gamma X$ coupling of the new particle to the photon, and $d_{1,s}$ depends on the spin of the particle. For instance, 2 TeV dilatons lead to $\zeta_1 \sim 10^{-13}$ GeV^{-4}. In Ref. [44], we performed an exact calculation and compared it with the usual effective Lagrangian approach and results were found to be similar.

The largest background to be considered to anomalous $\gamma\gamma\gamma\gamma$ events is the diphoton inclusive production (where the protons are destroyed in the final state) and intact protons detected in PPS originate from pile-up events. The number of pile-up events, or additional proton interactions within one bunch crossing, can reach 50 and will increase to 200 at the high-luminosity LHC. This means that we detect intact protons originating from pile-up every few bunch crossings. The fact that we measure all particles in the final state (the two γs and the two intact protons) allows for rejecting pile-up

background in a very efficient way, as shown in Fig. 17 [43]. For signal, the ratio of the diproton missing mass and the diphoton mass, and the difference between the diphoton and diproton rapidity should peak, respectively, around 1 and 0 within a detector resolution due to kinematics conservation. For pile-up, we expect a flat distribution since the diphotons and the diprotons do not originate from the same interaction. Requesting the matching between diphoton and diproton information allows for obtaining a negligible background for 300 fb^{-1}.

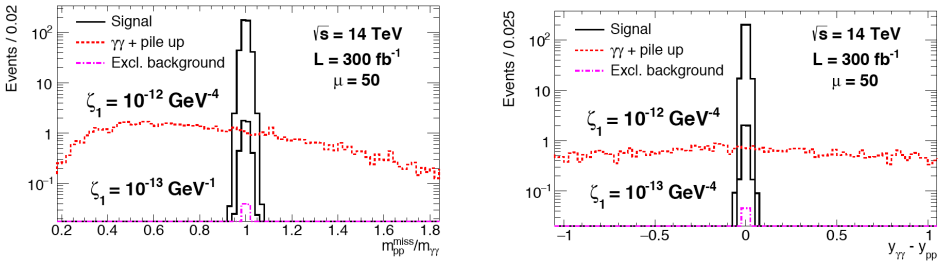

Fig. 17. Diffractive mass ratio and difference in rapidity using either the diphoton information from CMS or the proton taggings for signal in black and pile-up background in red.

Recently, the CMS Collaboration performed the search for exclusive diphoton production requesting two back-to-back photons at high diphoton mass ($m_{\gamma\gamma} > 350$ GeV), matching in rapidity and mass between the diphoton and diproton information. This led to the first limits on quartic photon anomalous couplings, $|\zeta_1| < 2.9 \times 10^{-13}$ GeV^{-4}, $|\zeta_2| < 6. \times 10^{-13}$ GeV^{-4} with about 10 fb^{-1} [45]. The limit was then updated with 102.7 fb^{-1} as $|\zeta_1| < 7.3 \times 10^{-14}$ GeV^{-4}, $|\zeta_2| < 1.5 \times 10^{-13}$ GeV^{-4} [45], as shown in Fig. 18, left. These results can be reinterpreted as a limit on ALPs at high masses and the results are shown in Fig. 18, right, as limits in the coupling *versus* mass plane. In Fig. 19, we also display the sensitivities projected for 300 fb^{-1} of luminosity [46]. The sensitivity for pp collisions is shown in a greyish area at high ALP mass, and we see that we gain about two orders of magnitude for ALP masses of about 1 TeV, and we reach an uncovered region at higher masses. It is also worth noting that the production of ALPs via photon exchanges in heavy-ion runs is complementary to the pp interactions and allows one to cover the intermediary region in ALP masses between a few GeV and 1 TeV. Heavy-ion runs show much lower luminosity than pp runs but the cross section is increased by Z^4 [46].

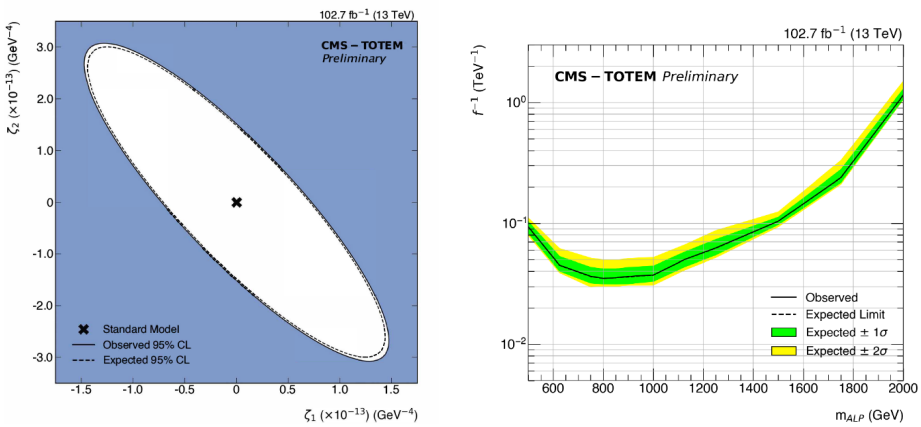

Fig. 18. Left: limits in the (ζ_1, ζ_2) plane for quartic anomalous $\gamma\gamma\gamma\gamma$ coupling. Right: Limits in the coupling *versus* mass plane for ALP production.

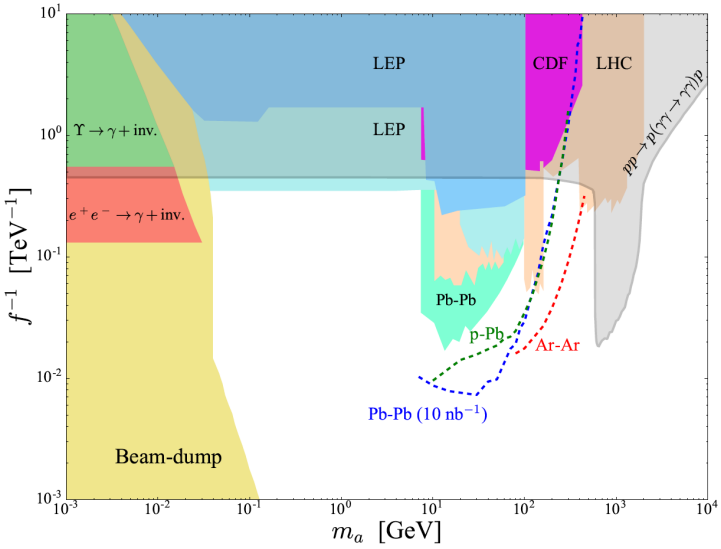

Fig. 19. Sensitivity plot in the coupling *versus* mass plane for ALP production for *pp* and heavy-ion interactions.

In Ref. [47], we also studied the sensitivity to quartic anomalous $\gamma\gamma\gamma Z$ coupling, considering the leptonic and hadronic Z-boson decays. The fact that we can control the background using the mass and rapidity matching technique allows us to look in both channels with negligible background. This leads to a very good sensitivity to $\gamma\gamma\gamma Z$ couplings, about three orders of magnitude better than the standard search at the LHC (looking for

the Z-boson decay into three photons is very challenging in a high pile-up environment). The advantage of our method is also that the sensitivity to anomalous couplings is performed in a model-independent way and the anomalous coupling can be due to wide or narrow resonances or loops of new particles as a threshold effect.

The CMS Collaboration also looked for quartic $\gamma\gamma WW$ and $\gamma\gamma ZZ$ anomalous couplings studying the case, where the W or Z bosons decay fully hadronically. This is because the anomalous production of WW/ZZ events dominates at high mass with a rather low cross section and the branching ratio into hadrons is higher. Two "fat" jets of radius 0.8 were selected with a transverse momentum $p_{\mathrm{T}} > 200$ GeV, a dijet mass $1126 < m_{jj} < 2500$ GeV, and the jets are requested to be back-to-back ($|1-\phi_{jj}/\pi| < 0.01$). As usual, the signal region is defined by the matching between the central WW system and the proton information. The results are shown in Fig. 20, left, and the limits on SM cross section are $\sigma_{WW} < 67$ fb, $\sigma_{ZZ} < 43$ fb for $0.04 < \xi < 0.2$ [48]. The new limits on quartic anomalous couplings with events violating unitarity removed are $a_0^W/\Lambda^2 < 4.3\times10^{-6}$ GeV^{-2}, $a_C^W/\Lambda^2 < 1.6\times10^{-5}$ GeV^{-2}, $a_0^Z/\Lambda^2 < 0.9\times10^{-5}$ GeV^{-2}, $a_C^Z/\Lambda^2 < 4.\times10^{-5}$ GeV^{-2} with 52.9 fb^{-1}. In Ref. [49], we also studied the possible observation of exclusive WW production with 300 fb^{-1} of data. The SM contribution appears at lower WW masses, as shown in Fig. 20, right, compared to anomalous couplings. This is why one needs to consider purely leptonic channels for W decays (the dijet background being too high at low masses for hadronic channels). The SM prediction on exclusive WW (leptonic decays) after selection is about 50 events for 300 fb^{-1} for a background estimate of 2 events.

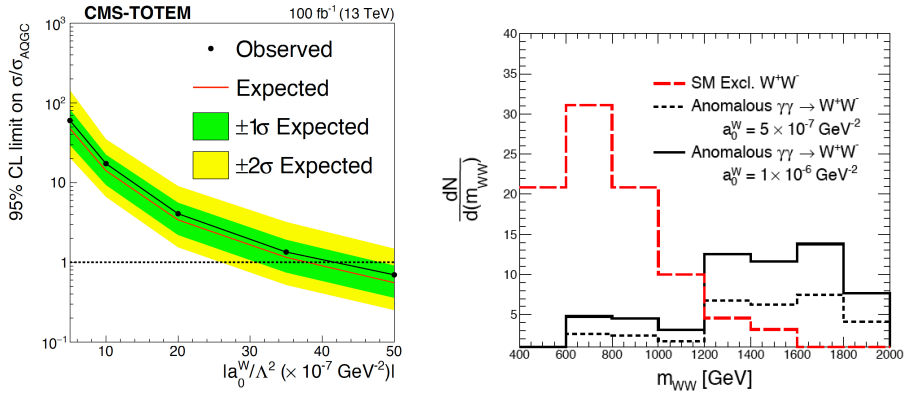

Fig. 20. Left: limits on a_0^W for quartic anomalous $\gamma\gamma WW$ coupling. Right: mass distribution for exclusive WW production for SM (red dashed line) and for two values of quartic anomalous $\gamma\gamma WW$ coupling (black full and dotted lines).

The CMS Collaboration also performed the search for exclusive $\gamma\gamma t\bar{t}$ processes in leptonic and semi-leptonic decays of top quarks with 29.4 fb^{-1} that led to a limit of $\sigma_{\rm excl} < 0.59$ pb [50]. A study concerning the sensitivity to $\gamma\gamma t\bar{t}$ quartic anomalous couplings was performed in Ref. [51] using a selection based on matching between the pp and $t\bar{t}$ information and on fast timing detectors to further suppress the pile-up background, and the sensitivity can reach 7×10^{-12} GeV^{-4} for 300 fb^{-1} of pp collisions using timing detectors with a resolution of about 20 ps.

In general, tagging protons at the LHC and matching the information of the tagged proton and the objects measured in the main CMS detector allow one to increase the sensitivity to $\gamma\gamma\gamma\gamma$, $\gamma\gamma WW$, $\gamma\gamma ZZ$, $\gamma\gamma\gamma Z$, $\gamma\gamma t\bar{t}$ quartic anomalous couplings by two or three orders of magnitude compared to more standard measurements at the LHC.

7. Conclusion

In this review, we presented first the discovery of the odderon by comparing the D0 $p\bar{p}$ and TOTEM pp elastic interactions. We then discussed the observation of gluon resummation effects at low x, especially in the measurement of the gap between jets and the possible observation of saturation in PbPb collision via the measurement of J/Ψ mesons, $c\bar{c}$ and $b\bar{b}$ production cross sections. We finished the report by discussing the sensitivity to quartic anomalous couplings and to the existence of ALPs by measuring intact protons at the LHC at high luminosity.

Many of these results originate from common work with long-term collaborators and I would like to thank all of them. I also thank Robi Peschanski for a careful reading of the manuscript.

REFERENCES

[1] H. Navelet, R. Peschanski, Ch. Royon, «Deep inelastic onium scattering», *Phys. Lett. B* **366**, 329 (1996); H. Navelet, R. Peschanski, Ch. Royon, S. Wallon, «Proton structure functions in the dipole picture of BFKL dynamics», *Phys. Lett. B* **385**, 357 (1996); A. Bialas, R. Peschanski, Ch. Royon, «Towards a unified description of total and diffractive structure functions at DESY HERA in the QCD dipole picture», *Phys. Rev. D* **57**, 6899 (1998); S. Munier, R. Peschanski, Ch. Royon, «Hard diffraction at HERA in the dipole model of BFKL dynamics», *Nucl. Phys. B* **534**, 297 (1998); M. Boonekamp, R. Peschanski, C. Royon, «Inclusive Higgs Boson and Dijet Production via Double Pomeron Exchange», *Phys. Rev. Lett.* **87**, 251806 (2001); M. Boonekamp, A. De Roeck, R. Peschanski, C. Royon, «Higgs boson production via double Pomeron exchange at the LHC», *Phys.*

Lett. B **550**, 93 (2002); M. Boonekamp, R. Peschanski, C. Royon, «Popping out the Higgs boson off vacuum at Tevatron and LHC», *Nucl. Phys. B* **669**, 277 (2003); M. Boonekamp, R. Peschanski, C. Royon, «Sensitivity to the standard model Higgs boson in exclusive double diffraction», *Phys. Lett. B* **598**, 243 (2004).

[2] D0 and TOTEM collaborations (V.M. Abazov *et al.*), «Odderon Exchange from Elastic Scattering Differences Between pp and $p\bar{p}$ Data at 1.96 TeV and from pp Forward Scattering Measurements», *Phys. Rev. Lett.* **127**, 062003 (2021).

[3] TOTEM Collaboration (G. Antchev *et al.*), «Performance of the Totem Detectors at the LHC», *Int. J. Mod. Phys. A* **28**, 1330046 (2013).

[4] ATLAS Collaboration (S.A. Khalek *et al.*), «The ALFA Roman Pot detectors of ATLAS», *J. Instrum.* **11**, P11013 (2016).

[5] D0 Collaboration (V.M. Abazov *et al.*), «The upgraded DØ detector», *Nucl. Instrum. Methods Phys. Res. A* **565**, 463 (2006).

[6] D0 Collaboration (V.M. Abazov *et al.*), «Measurement of the differential cross section $\mathrm{d}\sigma/\mathrm{d}t$ in elastic $p\bar{p}$ scattering at $\sqrt{s} = 1.96$ TeV», *Phys. Rev. D* **86**, 012009 (2012).

[7] TOTEM Collaboration (G. Antchev *et al.*), «Elastic differential cross-section $\mathrm{d}\sigma/\mathrm{d}t$ at $\sqrt{s} = 2.76$ TeV and implications on the existence of a colourless C-odd three-gluon compound state», *Eur. Phys. J. C* **80**, 91 (2020); «Proton–proton elastic scattering at the LHC energy of $\sqrt{s} = 7$ TeV», *Europhys. Lett.* **95**, 41004 (2011); «Evidence for non-exponential elastic proton–proton differential cross-section at low $|t|$ and $\sqrt{s} = 8$ TeV by TOTEM», *Nucl. Phys. B* **899**, 527 (2015); «Elastic differential cross-section measurement at $\sqrt{s} = 13$ TeV by TOTEM», *Eur. Phys. J. C* **79**, 861 (2019).

[8] L. Łukaszuk, B. Nicolescu, «A Possible Interpretation of pp Rising Total Cross-Sections», *Nuovo Cim. Lett.* **8**, 405 (1973).

[9] E. Martynov, B. Nicolescu, «Odderon effects in the differential cross-sections at Tevatron and LHC energies», *Eur. Phys. J. C* **79**, 461 (2019).

[10] F.E. Low, «Model of the bare Pomeron», *Phys. Rev. D* **12**, 163 (1975); S. Nussinov, «Colored-Quark Version of Some Hadronic Puzzles», *Phys. Rev. Lett.* **34**, 1286 (1975); P. Gauron, L. Łukaszuk, B. Nicolescu, «Consistency of the maximal odderon approach with the QFT constraints», *Phys. Lett. B* **294**, 298 (1992).

[11] A. Bouquet, B. Diu, E. Leader, B. Nicolescu, «A possible incompatibility between the $\mathcal{N}\mathcal{N}$ and $\bar{\mathcal{N}}\mathcal{N}$ total cross-sections and the Regge-pole modeltotal cross-sections and the Regge-pole model», *Nuovo Cim. A* **29**, 30 (1975); D. Joynson, E. Leader, B. Nicolescu, C. Lopez, «Non-regge and hyper-regge effects in pion–nucleon charge exchange scattering at high energies», *Nuovo Cim. A* **30**, 345 (1975); A.D. Donnachie, P.V. Landshoff, «Multi-gluon exchange in pp elastic scattering», *Phys. Lett. B* **123**, 345 (1983).

[12] J. Bartels, «High-energy behaviour in a non-abelian gauge theory (II). First corrections to $T_{n\to m}$ beyond the leading In s approximation», *Nucl. Phys. B* **175**, 365 (1980); J. Kwieciński, M. Praszałowicz, «Three gluon integral equation and odd C singlet Regge singularities in QCD», *Phys. Lett. B* **94**, 413 (1980).

[13] A. Breakstone *et al.*, «Measurement of $\bar{p}p$ and pp Elastic Scattering in the Dip Region at $\sqrt{s} = 53$ GeV», *Phys. Rev. Lett.* **54**, 2180 (1985); S. Erhan *et al.*, «Comparison $\bar{p}p$ of and pp elastic scattering with $0.6 < t < 2.1$ GeV^2 at the CERN-ISR», *Phys. Lett. B* **152**, 131 (1985); UA4 Collaboration (D. Bernard *et al.*), «Large-t elastic scattering at the CERN SPS collider at $\sqrt{s} = 630$ GeV», *Phys. Lett. B* **171**, 142 (1986); UA4 Collaboration (M. Bozzo *et al.*), «Elastic scattering at the CERN SPS collider up to a four-momentum transfer of 1.55 GeV^2», *Phys. Lett. B* **155**, 197 (1985); E. Nagy *et al.*, «Measurements of elastic proton–proton scattering at large momentum transfer at the CERN intersecting storage rings», *Nucl. Phys. B* **150**, 221 (1979).

[14] COMPETE Collaboration (J.R. Cudell *et al.*), «Benchmarks for the Forward Observables at RHIC, the Tevatron-Run II, and the LHC», *Phys. Rev. Lett.* **89**, 201801 (2002); V.A. Khoze. A.D. Martin, M.G. Ryskin, «Elastic and diffractive scattering at the LHC», *Phys. Lett. B* **784**, 192 (2018).

[15] TOTEM Collaboration (G. Antchev *et al.*), «First determination of the ρ parameter at $\sqrt{s} = 13$ TeV: probing the existence of a colourless C-odd three-gluon compound state», *Eur. Phys. J. C* **79**, 785 (2019).

[16] C. Baldenegro, C. Royon, A.M. Stasto, «Scaling properties of elastic proton–proton scattering at LHC energies», *Phys. Lett. B* **830**, 137141 (2022).

[17] C. Baldenegro, M. Praszałowicz, C. Royon, A.M. Staśto, «Scaling laws of elastic proton–proton scattering differential cross sections», *Phys. Lett. B* **856**, 138960 (2024).

[18] A.M. Staśto, K.J. Golec-Biernat, J. Kwieciński, «Geometric Scaling for the Total $\gamma^* p$ Cross Section in the Low x Region», *Phys. Rev. Lett.* **86**, 596 (2001); G. Beuf, R. Peschanski, C. Royon, D. Šálek, «Systematic analysis of scaling properties in deep inelastic scattering», *Phys. Rev. D* **78**, 074004 (2008).

[19] V.S. Fadin, E.A. Kuraev, L.N. Lipatov, «On the pomeranchuk singularity in asymptotically free theories», *Phys. Lett. B* **60**, 50 (1975); L.N. Lipatov, «Reggeization of the Vector Meson and the Vacuum Singularity in Nonabelian Gauge Theories», *Sov. J. Nucl. Phys.* **23**, 338 (1976); E.A. Kuraev, L.N. Lipatov, V.S. Fadin, «The Pomeranchuk Singularity in Nonabelian Gauge Theories», *Sov. Phys. JETP* **45**, 199 (1977); I.I. Balitsky, L.N. Lipatov, «The Pomeranchuk Singularity in Quantum Chromodynamics», *Sov. J. Nucl. Phys.* **28**, 822 (1978); V.S. Fadin, L.N. Lipatov, «BFKL pomeron in the next-to-leading approximation», *Phys. Lett. B* **429**, 127 (1998).

[20] G. Altarelli, G. Parisi, «Asymptotic freedom in parton language», *Nucl. Phys. B* **126**, 298 (1977); V.N. Gribov, L.N. Lipatov, «Deep inelastic *ep* scattering in perturbation theory», *Sov. J. Nucl. Phys.* **15**, 438 (1972); «e^+e^- pair annihilation and deep inelastic *ep* scattering in perturbation theory», *Sov. J. Nucl. Phys.* **15**, 675 (1972); Yu.L. Dokshitzer, «Calculation of structure functions of deep-inelastic scattering and e^+e^- annihilation by perturbation theory in quantum chromodynamic», *Sov. Phys. JETP.* **46**, 641 (1977).

[21] C. Marquet, R. Peschanski, C. Royon, «Saturation and forward jets at HERA», *Phys. Lett. B* **599**, 236 (2004); R. Peschanski, C. Royon, L. Schoeffel, «Confronting next-leading BFKL kernels with proton structure function data», *Nucl. Phys. B* **716**, 401 (2005); O. Kepka, C. Royon, C. Marquet, R. Peschanski, «Next-leading BFKL effects in forward-jet production at HERA», *Phys. Lett. B* **655**, 236 (2007);

[22] O. Kepka, C. Royon, C. Marquet, R. Peschanski, «Next-to-leading BFKL phenomenology of forward-jet cross sections at HERA», *Eur. Phys. J. C* **55**, 259 (2008).

[23] A.H. Mueller, H. Navelet, «An inclusive minijet cross section and the bare pomeron in QCD», *Nucl. Phys. B* **282**, 727 (1987); C. Marquet, C. Royon, «Azimuthal decorrelation of Mueller–Navelet jets at the Tevatron and the LHC», *Phys. Rev. D* **79**, 034028 (2009); O. Kepka, C. Royon, C. Marquet, R. Peschanski, «Next-leading BFKL effects in forward-jet production at HERA», *Phys. Lett. B* **655**, 236 (2007); C. Marquet, C. Royon, «Small-x QCD effects in forward-jet and Mueller–Navelet jet production», *Nucl. Phys. B* **739**, 131 (2006); C. Marquet, R. Peschanski, C. Royon, «Saturation and forward jets at HERA», *Phys. Lett. B* **599**, 236 (2004).

[24] F. Deganutti, C. Royon, S. Schlichting, «Forward dijet production at the LHC within an impact parameter dependent TMD approach», *J. High Energy Phys.* **2024**, 159 (2024).

[25] CMS Collaboration, «Hard color-singlet exchange in dijet events in proton–proton collisions at $\sqrt{s} = 13$ TeV», *Phys. Rev. D* **104**, 032009 (2021); O. Kepka, C. Marquet, C. Royon, «Gaps between jets in hadronic collisions», *Phys. Rev. D* **83**, 034036 (2011); F. Chevallier, O. Kepka, C. Marquet, C. Royon, «Gaps between jets at hadron colliders in the next-to-leading BFKL framework», *Phys. Rev. D* **79**, 094019 (2009).

[26] C. Baldenegro *et al.*, «Jets separated by a large pseudorapidity gap at the Tevatron and at the LHC», *J. High Energy Phys.* **2022**, 250 (2022).

[27] T. Sjöstrand *et al.*, «An introduction to PYTHIA 8.2», *Comput. Phys. Commun.* **191**, 159 (2015).

[28] D. Colferai, F. Deganutti, T.G. Raben, C. Royon, «First computation of Mueller Tang processes using a full NLL BFKL approach», *J. High Energy Phys.* **2023**, 91 (2023).

[29] C. Marquet, C. Royon, M. Trzebiński, R. Žlebčík, «Gaps between jets in double-Pomeron-exchange processes at the LHC», *Phys. Rev. D* **87**, 034010 (2013).

[30] Y.V. Kovchegov, «Small-x F_2 structure function of a nucleus including multiple Pomeron exchanges», *Phys. Rev. D* **60**, 034008 (1999); I. Balitsky, «Operator expansion for high-energy scattering», *Nucl. Phys. B* **463**, 99 (1996).

[31] J. Penttala, C. Royon, «Gluon saturation effects in exclusive heavy vector meson photoproduction», *Phys. Lett. B* **864**, 139394 (2025).

[32] H. Mäntysaari, J. Penttala, F. Salazar, B. Schenke, «Finite-size effects on small-x evolution and saturation in proton and nuclear targets», *Phys. Rev. D* **111**, 054033 (2025).

[33] H1 Collaboration (A. Aktas *et al.*), «Elastic J/Ψ production at HERA», *Eur. Phys. J. C* **46**, 585 (2006); H1 Collaboration (C. Alexa *et al.*), «Elastic and proton-dissociative photoproduction of J/Ψ mesons at HERA», *Eur. Phys. J. C* **73**, 2466 (2013); H1 Collaboration (C. Adloff *et al.*), «Elastic photoproduction of J/Ψ and Υ mesons at HERA», *Phys. Lett. B* **483**, 23 (2000).

[34] ZEUS Collaboration (S. Chekanov *et al.*), «Exclusive photoproduction of J/ψ mesons at HERA», *Eur. Phys. J. C* **24**, 345 (2002); ZEUS Collaboration (J. Breitweg *et al.*), «Measurement of elastic Υ photoproduction at HERA», *Phys. Lett. B* **437**, 432 (1998); ZEUS Collaboration (S. Chekanov *et al.*), «Exclusive photoproduction of Υ mesons at HERA», *Phys. Lett. B* **680**, 4 (2009).

[35] CMS Collaboration (A. Tumasyan *et al.*), «Probing Small Bjorken-x Nuclear Gluonic Structure via Coherent J/ψ Photoproduction in Ultraperipheral Pb–Pb Collisions at $\sqrt{s_{NN}} = 5.02$ TeV», *Phys. Rev. Lett.* **131**, 262301 (2023); CMS Collaboration (A.M. Sirunyan *et al.*), «Measurement of exclusive Υ photoproduction from protons in pPb collisions at $\sqrt{s_{NN}} = 5.02$ TeV», *Phys. J. C* **79**, 277 (2019).

[36] ALICE Collaboration (S. Acharya *et al.*), «Energy dependence of coherent photonuclear production of J/Ψ mesons in ultra-peripheral Pb–Pb collisions at $\sqrt{s_{NN}} = 5.02$ TeV», *J. High Energy Phys.* **2023**, 119 (2023); ALICE Collaboration (B. Abelev *et al.*), «Exclusive J/ψ Photoproduction off Protons in Ultraperipheral p–Pb Collisions at $\sqrt{s_{NN}} = 5.02$ TeV», *Phys. Rev. Lett.* **113**, 232504 (2014); ALICE Collaboration (S. Acharya *et al.*), «Energy dependence of exclusive J/ψ photoproduction off protons in ultra-peripheral p–Pb collisions at $\sqrt{s_{NN}} = 5.02$ TeV», *Eur. Phys. J. C* **79**, 402 (2019).

[37] LHCb Collaboration (R. Aaij *et al.*), «Central exclusive production of J/Ψ and $\Psi(2S)$ mesons in pp collisions at $\sqrt{s} = 13$ TeV», *J. High Energy Phys.* **2018**, 167 (2018); «Updated measurements of exclusive J/Ψ and $\Psi(2S)$ production cross-sections in pp collisions at $\sqrt{s} = 7$ TeV», *J. Phys. G: Nucl. Part. Phys.* **41**, 055002 (2014); «Measurement of the exclusive Υ production cross-section in pp collisions at $\sqrt{s} = 7$ TeV and 8 TeV», *J. High Energy Phys.* **2015**, 084 (2015).

[38] CMS Collaboration, «First measurement of coherent photoproduction of $\Upsilon(1S)$ mesons in lead–lead ultraperipheral collisions at $\sqrt{s} = 5.02$ TeV», report No. CMS-PAS-HIN-24-013.

[39] J. Penttala, C. Royon, J. Vierros, in preparation.

[40] C. Marquet, C. Royon, M. Saimpert, D. Werder, «Probing the Pomeron structure using dijets and $\gamma +$ jet events at the LHC», *Phys. Rev. D* **88**, 074029 (2013); C. Marquet *et al.*, «Diffractive di-jet production at the LHC with a Reggeon contribution», *Phys. Lett. B* **766**, 23 (2017); A. Chuinard, C. Royon, R. Staszewski, «Testing Pomeron flavour symmetry with diffractive W charge asymmetry», *J. High Energy Phys.* **2016**, 092 (2016); K. Golec-Biernat, C. Royon, L. Schoeffel, R. Staszewski, «Electroweak vector boson production at the LHC as a probe of mechanisms of diffraction», *Phys. Rev. D* **84**, 114006 (2011).

[41] CMS and TOTEM collaborations, «CMS–TOTEM Precision Proton Spectrometer», report No. CERN-LHCC-2014-021, TOTEM-TDR-003, CMS-TDR-013.

[42] ATLAS Collaboration, «Technical Design Report for the ATLAS Forward Proton Detector», report No. CERN-LHCC-2015-009, ATLAS-TDR-024.

[43] S. Fichet *et al.*, «Probing new physics in diphoton production with proton tagging at the Large Hadron Collider», *Phys. Rev. D* **89**, 114004 (2014); O. Kepka, E. Chapon, C. Royon, «Anomalous quartic $WW\gamma\gamma$, $ZZ\gamma\gamma$, and trilinear $WW\gamma$ couplings in two-photon processes at high luminosity at the LHC», *Phys. Rev. D* **81**, 074003 (2010); S. Fichet, G. von Gersdorff, C. Royon, «Scattering light by light at 750 GeV at the LHC», *Phys. Rev. D* **93**, 075031 (2016); O. Kepka, C. Royon, «Anomalous $WW\gamma$ coupling in photon-induced processes using forward detectors at the CERN LHC», *Phys. Rev. D* **78**, 073005 (2008); S. Fichet, G. von Gersdorff, C. Royon, «Measuring the Diphoton Coupling of a 750 GeV Resonance», *Phys. Rev. Lett.* **116**, 231801 (2016).

[44] S. Fichet *et al.*, «Light-by-light scattering with intact protons at the LHC: from standard model to new physics», *J. High Energy Phys.* **2015**, 165 (2015).

[45] CMS and TOTEM collaborations (A. Tumasyan *et al.*), «First Search for Exclusive Diphoton Production at High Mass with Tagged Protons in Proton–Proton Collisions at $\sqrt{s} = 13$ TeV», *Phys. Rev. Lett.* **129**, 011801 (2022); «Search for high-mass exclusive diphoton production with tagged protons in proton–proton collisions at $\sqrt{s} = 13$ TeV», *Phys. Rev. D* **110**, 012010 (2024).

[46] C. Baldenegro, S. Fichet, G. von Gersdorff, C. Royon, «Searching for axion-like particles with proton tagging at the LHC», *J. High Energy Phys.* **2018**, 131 (2018); C. Baldenegro, S. Hassani, C. Royon, L. Schoeffel, «Extending the constraint for axion-like particles as resonances at the LHC and laser beam experiments», *Phys. Lett. B* **795**, 339 (2019); D. d'Enterria, G.G. da Silveira, «Observing Light-by-Light Scattering at the Large Hadron Collider», *Phys. Rev. Lett.* **111**, 080405 (2013).

[47] C. Baldenegro, S. Fichet, G. von Gersdorff, C. Royon, «Probing the anomalous $\gamma\gamma\gamma z$ coupling at the LHC with proton tagging», *J. High Energy Phys.* **2017**, 142 (2017).

[48] CMS and TOTEM collaborations (A. Tumasyan *et al.*), «Search for high-mass exclusive $\gamma\gamma \to WW$ and $\gamma\gamma \to ZZ$ production in proton–proton collisions at $\sqrt{s} = 13$ TeV», *J. High Energy Phys.* **2023**, 229 (2023).

[49] C. Baldenegro, G. Biagi, G. Legras, C. Royon, «Central exclusive production of W boson pairs in pp collisions at the LHC in hadronic and semi-leptonic final states», *J. High Energy Phys.* **2020**, 165 (2020).

[50] CMS and TOTEM collaborations (A. Tumasyan *et al.*), «Search for central exclusive production of top quark pairs in proton–proton collisions at $\sqrt{s} = 13$ TeV with tagged protons», *J. High Energy Phys.* **2024**, 187 (2024).

[51] C. Baldenegro *et al.*, «Searching for anomalous top quark interactions with proton tagging and timing detectors at the LHC», *J. High Energy Phys.* **2022**, 21 (2022).